ChemPubSoc Europe

DOI: 10.1002/ejic.201900595

EurJIC European Journal of Inorganic Chemistry

Full Paper

Molybdenum Fluorides

Lewis Acidic Behavior of $MoOF_4$ towards the Alkali Metal Fluorides in Anhydrous Hydrogen Fluoride Solutions

Riane E. Stene,[a,b] Benjamin Scheibe,[a] Antti J. Karttunen,[c] Winfried Petry,[b] and Florian Kraus*[a]

Abstract: Previous studies performed on samples of $MoOF_4$ dissolved in anhydrous hydrogen fluoride (aHF) solutions have indicated the presence of the $[Mo_2O_2F_9]^-$ anion. Building upon this earlier work, $MoOF_4$, and *M*F (*M* = Li–Cs) were dissolved in aHF solutions to produce $M[Mo_2O_2F_9]$ (*M* = Li–Cs) salts. Structural analysis of the obtained compounds was performed using single-crystal X-ray diffraction. This study provides the first single crystal structures for the $[Mo^{VI}_2O_2F_9]^-$ anion. Additionally, IR and Raman spectroscopy were used to characterize each salt. These spectra were compared to calculated ones for the solid-state structure of each salt using the DFT-PBE0 density functional method. The calculated spectra were used to give band assignments in the experimentally obtained spectra.

Introduction

Trifluorido trioxido molybdate(VI) anions, $[MoO_3F_3]^{3-}$, such as those in $K_3MoO_3F_3$ and $Cs_2RbMoO_3F_3$, have been shown to display many applicable physical properties, most notably ferroelectricity.[1,2] In addition, molybdenum oxide fluoride anions, in which the molybdenum atoms have d^0 electronic configurations, may exhibit second-order Jahn–Teller distortion.[3] This distortion, characterized by a displacement of the Mo atom from the center of its octahedral coordination environment, and alternating atomic distances between the Mo and neighboring bridging fluorine/oxygen atoms, can yield compounds displaying metallic, ferroelectric, and magnetic behaviors.[3] In order to exploit potential promising physical and chemical properties, many molybdenum oxide fluorides have been synthesized to date.[4–8] However, little remains known regarding the chemical properties of the simplest Mo^{VI} molybdenum oxide fluoride, $MoOF_4$.

$MoOF_4$ was first synthesized in 1907 by Ruff and Eisner, whereby aHF was condensed onto molybdenum oxide tetrachloride ($MoOCl_4$).[9] $MoOF_4$ is a white solid having a melting point of 97 °C and a boiling point of 186 °C (under ambient atmospheric pressure).[9] The crystal structure of $MoOF_4$, which is related to that of VF_5,[10] is characterized by essentially octahedrally-coordinated Mo atoms linked into infinite chains by *cis*-bridging fluorine atoms.[11] The solid-state structure of $MoOF_4$ features Mo atoms in distorted octahedral surroundings and alternating Mo–(μ-F) atomic distances, see Figure 1.[3]

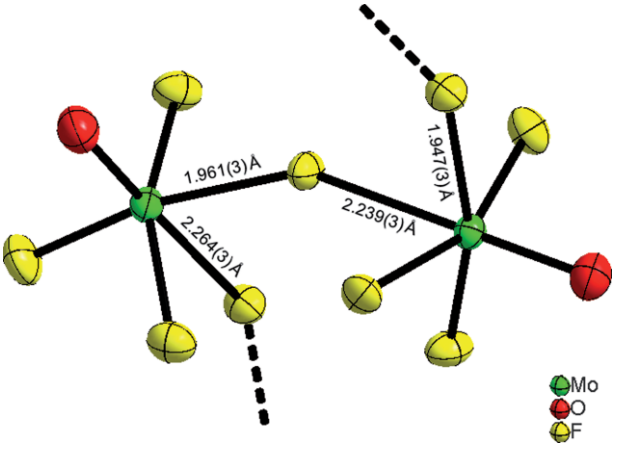

Figure 1. Section of the infinite, one-dimensional chains observed in the solid-state structure of $MoOF_4$. Atomic distances between Mo and the μ-F atoms are displayed to show their alternating pattern. Displacement ellipsoids are shown at a 70 % probability level at 100 K.

$MoOF_4$ has been described in the literature as being a weak Lewis acid and fluoride ion acceptor, with WOF_4 being, comparatively, both a stronger Lewis acid and fluoride ion acceptor.[12,13] A detailed understanding of the Lewis acid and fluoride ion acceptor behavior of $MoOF_4$ in aHF was given by Bougon and co-workers, who studied aHF solutions containing $MoOF_4$ and fluoride ion donors using Raman and ^{19}F NMR spectroscopy.[12] Their study determined that $MoOF_4$ forms a chemical equilibrium in aHF solutions between the $[Mo_2O_2F_9]^-$, $[MoOF_5]^-$, $[MoOF_6]^{2-}$ anions, depending on the $[HF_2]^-$ concentration available in solution, as shown in Equations 1–3.[12] It was predicted that higher concentrations of $[HF_2]^-$ drives the chemical equilibrium of each reaction to the right, and thus

[a] *Anorganische Chemie, Fachbereich Chemie, Phillips-Universität Marburg, Hans-Meerwein-Straße 4, 35032 Marburg, Germany*
E-mail: florian.kraus@chemie.uni-marburg.de
[b] *Neutron Research Source Heinz Maier-Leibnitz (FRM II), Technische Universität München, Lichtenbergstraße 1 85748 Garching, Germany*
[c] *Department of Chemistry and Material Science, Aalto University, 00076 Aalto, Finland*
Supporting information and ORCID(s) from the author(s) for this article are available on the WWW under https://doi.org/10.1002/ejic.201900595.

pushes the chemical equilibrium from the left side of Equation 1 to the right side of Equation 3.[12]

$$2\ MoOF_4 + [HF_2]^- \overset{aHF}{\rightleftharpoons} [Mo_2O_2F_9]^- + HF \quad (1)$$

$$[Mo_2O_2F_9]^- + [HF_2]^- \overset{aHF}{\rightleftharpoons} 2\ [MoOF_5]^- + HF \quad (2)$$

$$[MoOF_5]^- + [HF_2]^- \overset{aHF}{\rightleftharpoons} [MoOF_6]^{2-} + HF \quad (3)$$

Similarly, a study aimed at determining the interaction of $MoOF_4$ with acetylacetone in acetonitrile solution also reported evidence for the formation of the $[Mo_2O_2F_9]^-$ anion.[14] Additionally, work performed by Holloway and Schrobilgen described the formation of $KrF_2{\cdot}nMoF_4$ (n = 1–3) and $XeF_2{\cdot}nMoOF_4$ (n = 1–4) adducts, in which a structurally related anion, MoO_2F_8, to which an F atom from a XeF_2 ligand is bound, was observed.[13,15] These studies shed much light on the complex equilibria and solution chemistry $MoOF_4$ can exhibit.[12–15] However, despite the potential of $MoOF_4$ to give rise to new chemical species, very little literature exists in which $MoOF_4$ was used as a starting reagent in chemical reactions.[12–22] Therefore, the goal of this work was to expand the current knowledge of the chemical behavior of $MoOF_4$ in aHF solutions by reacting it with the alkali metal fluorides. As a result, the series of $M[Mo_2O_2F_9]$ (M = Li–Cs) salts was obtained. Structural analysis of these salts, performed using single-crystal X-ray diffraction, provides the first crystal structures containing the $[Mo^{VI}{}_2O_2F_9]^-$ anion. The structures of these anions will be compared to the previously reported $[Mo^{V}{}_2O_2F_9]^{3-}$ anions. Furthermore, vibrational spectroscopy was studied using IR and Raman techniques and the obtained spectra were compared to quantum chemically calculated solid-state spectra. A discussion on the synthesis of the $M[Mo_2O_2F_9]$ (M = Li–Cs) salts is presented, along with suggestions as to the possible synthesis of $M[MoOF_5]$ and $M_2[MoOF_6]$ (M = Li–Cs) salts.

Results and Discussion

Synthesis of the $M[Mo_2O_2F_9]$ (M = Li–Cs) Salts

First, $MoOF_4$ was synthesized through the hydrolysis of MoF_6 by silicon dioxide in aHF, see Equations 4 and 5.[23] After pumping off the unreacted aHF and the SiF_4 formed during the reaction, the $MoOF_4$ product was stored in an inert atmosphere glovebox until further use. Next, a 1:1 molar ratio of $MoOF_4$ and the respective alkali metal fluoride was reacted in an aHF solution to obtain the $M[Mo_2O_2F_9]$ (M = Li–Cs) salts, see Equation 6. Single crystals of the salts were grown directly from aHF solution. However, as evidenced by X-ray powder diffraction, as well as IR and Raman spectroscopy, the compounds could not be obtained phase-pure. Evidence suggests the impurities to be

$$SiO_2 + 4\ HF \xrightarrow{aHF} SiF_4 + 2\ H_2O \quad (4)$$

$$MoF_6 + H_2O \xrightarrow{HF} MoOF_4 + 2\ HF \quad (5)$$

$$2\ MoOF_4 + MF \xrightarrow{aHF} M[Mo_2O_2F_9] \quad (6)$$

Table 1. Selected crystallographic data and details of the single crystal structure determination for the $M[Mo_2O_2F_9]$ (M = Li–Cs) salts.

	Li[$Mo_2O_2F_9$]	Na[$Mo_2O_2F_9$]	K[$Mo_2O_2F_9$]	Rb[$Mo_2O_2F_9$]	Cs[$Mo_2O_2F_9$]
Empirical formula	$F_9LiMo_2O_2$	$F_9Mo_2NaO_2$	$F_9KMo_2O_2$	$F_9Mo_2O_2Rb$	$CsF_9Mo_2O_2$
Color and appearance	colorless blocks	colorless blocks	colorless blocks	colorless blocks	colorless blocks
Molar mass /g mol^{-1}	401.82	417.87	433.98	480.35	527.79
Crystal system	triclinic	monoclinic	monoclinic	monoclinic	monoclinic
Space group type (No.)	$P\bar{1}$ (2)	$P2/c$ (13)	$P2/c$ (13)	$P2/c$ (13)	$P2/c$ (13)
Pearson symbol	$aP28$	$mP28$	$mP28$	$mP28$	$mP28$
a /Å	5.0871(2)	8.1441(8)	5.4386(4)	5.6244(3)	5.9162(3)
b /Å	8.4456(4)	6.5008(4)	5.0712(3)	5.1946(2)	5.4203(3)
c /Å	10.0254(4)	8.6741(8)	15.1497(10)	14.9973(8)	14.7154(7)
α /°	66.432(3)	••	••	••	••
β /°	77.268(4)	113.025(7)	105.842(6)	106.748(5)	108.554(4)
γ /°	89.436(4)	••	••	••	••
V /Å^3	383.61(3)	422.65(7)	401.96(5)	419.58(4)	447.36(4)
Z	2	2	2	2	2
$\rho_{calcd.}$ /g cm^{-3}	3.479	3.284	3.586	3.802	3.918
λ /Å	0.71073 (Mo-K_α)				
T /K	100				
μ /mm^{-1}	3.41	3.14	3.77	8.88	6.93
θ_{max}	33.4	33.3	28.7	33.3	32.0
hkl_{range}	$-7 \le h \le 7$	$-12 \le h \le 12$	$-7 \le h \le 7$	$-8 \le h \le 8$	$-8 \le h \le 8$
	$-13 \le k \le 13$	$-10 \le k \le 10$	$-6 \le k \le 6$	$-8 \le k \le 8$	$-8 \le k \le 8$
	$-15 \le l \le 15$	$-11 \le l \le 13$	$-20 \le l \le 19$	$-23 \le l \le 23$	$-20 \le l \le 21$
R_{int}, R_σ	0.075, 0.043	0.093, 0.042	0.043, 0.032	0.110, 0.053	0.030, 0.015
$R(F)$ [$I \ge 2\sigma(I)$, all data]	0.036, 0.051	0.057, 0.074	0.019, 0.037	0.030, 0.032	0.026, 0.030
$wR(F^2)$ [$I \ge 2\sigma(I)$, all data]	0.066, 0.072	0.112, 0.120	0.033, 0.036	0.063, 0.064	0.063, 0.064
S (all data)	1.10	1.14	1.01	1.10	1.26
Data, parameter, restraints	2949, 134, 0	1640, 65, 0	1039, 66, 0	1625, 66, 0	1556, 65, 0
$\Delta\rho_{max}$, $\Delta\rho_{min}$ /e Å^{-3}	1.25, –1.36	1.40, –2.15	0.54, –0.68	1.07, –1.93	1.43, –2.17

the respective adducts of $[F(HF)_n]$ (n = 1,2)], and other, yet unidentified, compounds.

Single Crystal X-ray Analysis

All $M[Mo_2O_2F_9]$ (M = Li–Cs) salts contain $[Mo_2O_2F_9]^-$ anions surrounded by several of the respective alkali metal cations. The $[Mo_2O_2F_9]^-$ anion can be thought of as two $MoOF_4$ units bridged by a fluoride anion, as shown in Figure 2. The anion may be described by the Niggli formula $_\infty^0\{[MoO_{1/1}F_{4/1}F_{1/2}]^{0.5-}\}_2$. Selected crystallographic data and details of the single crystal structure determination are given in Table 1. The single crystal structures of each salt will be discussed individually; comparisons, when appropriate, will be noted. A comparison of the salts reported here to the previously reported $(NH_4)_3[Mo^V_2O_2F_9]$ and $K_2(NMe_4)[Mo^V_2O_2F_9]{\cdot}H_2O$ salts will be presented at the end of this section.

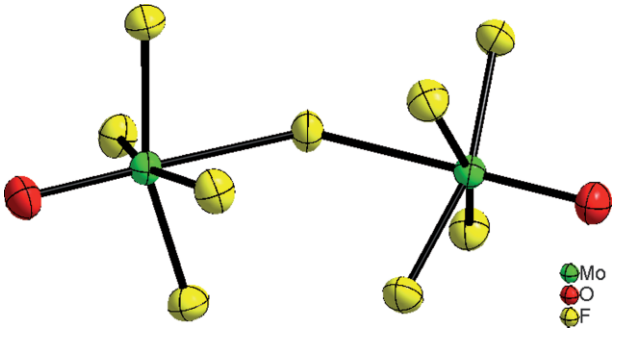

Figure 2. The $[Mo_2O_2F_9]^-$ anion observed in $Rb[Mo_2O_2F_9]$. Displacement ellipsoids are shown at a 70 % probability level at 100 K.

1. Single Crystal Structure of $Li[Mo_2O_2F_9]$

$Li[Mo_2O_2F_9]$ crystallizes in the triclinic space group $P\bar{1}$ with the lattice parameters a = 5.0871(2), b = 8.4456(4), c = 10.0254(4) Å, α = 66.432(3), β = 77.268(4), γ = 89.436(4)°, V = 383.61(3) Å^3, Z = 2, T = 100 K. Atomic coordinates and equivalent isotropic displacement parameters for $Li[Mo_2O_2F_9]$ are reported in Table 2. The unit cell contains two symmetrically inequivalent $[Mo_2O_2F_9]^-$ anions coordinating to two distinct Li^+ cations. Li(1) has full site occupancy and is octahedrally coordinated by six terminal fluorine atoms (F_t) belonging to four $[Mo_2O_2F_9]^-$ anions (Figure S1). On the other hand, Li(2) experiences disorder due to space group symmetry (center of inversion) and its site occupancy factor was fixed to a value of 0.5. The Li(2) cation is coordinated by four F_t atoms also belonging to four $[Mo_2O_2F_9]^-$ anions, forming a tetrahedral coordination polyhedron (Figure S2a). The coordination tetrahedron around Li(2) shares an edge with the coordination tetrahedron generated by the crystallographic inversion center (Figure S2b). Similar edge-sharing tetrahedra containing disordered Li^+ cations have been described previously in compounds such as Li_3InF_6,[24] Li_7OsO_6,[25] and $Li_9B_{19}S_{33}$.[26] Moreover, the coordination of the $[Mo_2O_2F_9]^-$ anions to the lithium cations form two-dimensional infinite sheets, which are oriented parallel to the (011) plane, see Figure S3 (for a topological comparison of the crystal structures, see below).

Table 2. Atomic coordinates and equivalent isotropic displacement parameters U_{iso} for $Li[Mo_2O_2F_9]$.

Atom	Position	x	y	z	U_{iso} /Å^2
Mo(1)	2*i*	0.13030(6)	0.02600(4)	0.21547(3)	0.01007(8)
Mo(2)	2*i*	0.16784(6)	0.54561(4)	0.71704(3)	0.01090(8)
F(000)	2*i*	0.0190(5)	0.2704(3)	0.2089(3)	0.0173(4)
F(2)	2*i*	0.3716(4)	0.0654(3)	0.3193(2)	0.0149(4)
F(3)	2*i*	0.3681(5)	0.1676(3)	0.0370(2)	0.0176(4)
F(4)	2*i*	0.8591(5)	0.0382(3)	0.1194(3)	0.0202(5)
F(5)	2*i*	0.1320(4)	0.0507(3)	0.6034(2)	0.0150(4)
F(6)	2*i*	0.0744(5)	0.6040(3)	0.1106(3)	0.0174(4)
F(7)	2*i*	0.0966(5)	0.4190(3)	0.3876(3)	0.0179(4)
F(8)	2*i*	0.6307(4)	0.2556(3)	0.4345(2)	0.0145(4)
F(9)	2*i*	0.6051(5)	0.4503(3)	0.1575(3)	0.0194(5)
O(1)	2*i*	0.2293(6)	0.8352(4)	0.2272(3)	0.0181(5)
O(2)	2*i*	0.3227(6)	0.3989(4)	0.6656(3)	0.0207(6)
Li(1)	1*c*	1/2	0	1/2	0.0203(19)
Li(2)	2*i*	0.440(3)	0.607(2)	0.0021(18)	0.023(3)

When the $[Mo_2O_2F_9]^-$ anion is viewed from the side, so that the respective Mo atoms are eclipsing, it can be seen that the adjacent F_t atoms are nearly eclipsing. The smallest of these

Table 3. Selected interatomic distances and angles in the $M[Mo_2O_2F_9]$ (M = Li–Cs) salts. In the case of $Li[Mo_2O_2F_9]$, all atomic distances reported have a multiplicity of 1; for $M[Mo_2O_2F_9]$ (M = Na–Cs), all reported atomic distances have a multiplicity of 2.

Interatomic distances /Å	$Li[Mo_2O_2F_9]$	$Na[Mo_2O_2F_9]$	$K[Mo_2O_2F_9]$	$Rb[Mo_2O_2F_9]$	$Cs[Mo_2O_2F_9]$
Mo(1)–μ-F(1)	2.114(2)	2.1489(15)	2.1607(8)	2.1624(7)	2.1509(14)
Mo(1)–F(2)	1.884(2)	1.871(4)	1.8598(17)	1.8649(14)	1.860(3)
Mo(1)–F(3)	1.873(2)	1.860(4)	1.8485(16)	1.8547(14)	1.849(3)
Mo(1)–F(4)	1.829(2)	1.828(4)	1.8524(17)	1.8553(14)	1.847(3)
Mo(1)–F(5)	1.860(2)	1.859(4)	1.8569(16)	1.8580(14)	1.855(3)
Mo(1)–O(1)	1.650(3)	1.660(5)	1.646(2)	1.6522(17)	1.651(3)
Mo(2)–μ-F(1)	2.110(2)	–	–	–	–
Mo(2)–F(6)	1.895(2)	–	–	–	–
Mo(2)–F(7)	1.867(2)	–	–	–	–
Mo(2)–F(8)	1.834(2)	–	–	–	–
Mo(1)–F(9)	1.857(2)	–	–	–	–
Mo(1)–O(2)	1.653(3)	–	–	–	–
Interatomic angles /°					
Mo(1)–μ-F(1)–Mo(1)	–	150.7(3)	137.98(11)	138.89(10)	140.7(2)
Mo(1)–μ-F(1)–Mo(2)	158.89(12)	–	–	–	–

torsion angles range between 2.393(11)° and 6.781(12)°. Upon comparison of the torsion angles between F_t atoms in the $M[Mo_2O_2F_9]$ (M = Na–Cs) salts, a trend became apparent: the larger the respective cation, the larger the respective torsion angles. That is, nearly eclipsing F_t atoms were observed in $Li[Mo_2O_2F_9]$ while a more staggered conformation of F_t atoms was observed in $Cs[Mo_2O_2F_9]$. A schematic showing the differences in torsion angle can be seen in Figure S4. A complete list of torsion angles observed in $Li[Mo_2O_2F_9]$ is reported in Table S1. A list of selected atomic distances and angles observed in the $M[Mo_2O_2F_9]$ (M = Li–Cs) salts is reported in Table 3.

In comparison to the other salts reported here, $Li[Mo_2O_2F_9]$ has the largest range for its Mo–F_t atomic distances, ranging from 1.829(2) to 1.895(2) Å. Additionally, the shortest Mo–μ-F atomic distances were observed in $Li[Mo_2O_2F_9]$, ranging from 2.110(2) to 2.114(2) Å. The Mo–O atomic distances in $Li[Mo_2O_2F_9]$ have values of 1.650(3) and 1.653(3) Å and the Mo–F_μ–Mo angle in the lithium salt was observed to be 158.89(12)°; the largest Mo–μ-F–Mo angle in the series. A section of the crystal structure of $Li[Mo_2O_2F_9]$ is shown in Figure 3. To the best of our knowledge, the compound represents a new structure type.

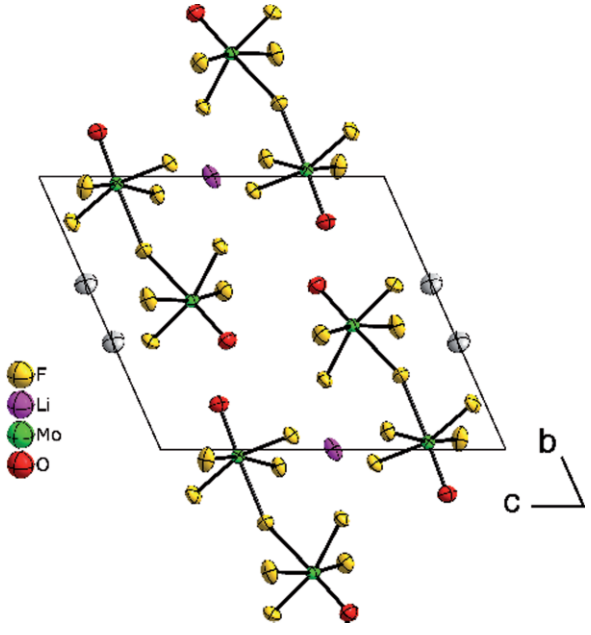

Figure 3. Section of the crystal structure of $Li[Mo_2O_2F_9]$. Displacement ellipsoids are shown at a 70 % probability level at 100 K, grey atoms indicate Li atoms with site disorder.

2. Single Crystal Structure of $Na[Mo_2O_2F_9]$

$Na[Mo_2O_2F_9]$ crystallizes in the monoclinic space group $P2/c$ with the lattice parameters a = 8.14411(8), b = 6.5008(4), c = 8.6741(8) Å, β = 113.025(7)°, V = 422.65(7) Å^3, Z = 2, T = 100 K. Atomic coordinates and equivalent isotropic displacement parameters for $Na[Mo_2O_2F_9]$ are reported in Table 4. The coordination number of the sodium cation is seven as a result of six coordinating F_t atoms and one coordinating μ-F atom (belonging to four different $[Mo_2O_2F_9]^-$ anions), creating a distorted pentagonal bipyramidal coordination polyhedron (Figure S5). The coordination of the $[Mo_2O_2F_9]^-$ anions to the sodium cations again leads to the formations of two-dimensional infinite sheets which are parallel to the b–c plane, see Figure S6.

Table 4. Atomic coordinates and equivalent isotropic displacement parameters U_{iso} for $Na[Mo_2O_2F_9]$.

Atom	Position	x	y	z	U_{iso} /Å^2
Mo(1)	4*g*	0.25927(6)	0.76012(7)	0.43034(6)	0.01342(13)
F(1)	2*e*	0	0.6764(8)	1/4	0.0208(11)
F(2)	4*g*	0.2791(6)	0.4755(6)	0.4260(6)	0.0266(9)
F(3)	4*g*	0.1433(6)	0.2804(7)	0.0763(5)	0.0267(9)
F(4)	4*g*	0.1647(6)	0.0246(6)	0.3934(6)	0.0276(10)
F(5)	4*g*	0.3084(7)	0.2154(10)	0.7429(6)	0.0394(13)
O(1)	4*g*	0.4602(7)	0.1857(7)	0.0735(6)	0.0218(9)
Na(1)	2*e*	0	0.3027(5)	1/4	0.0176(7)

The smallest torsion angles between adjacent F_t atoms (seen when the $[Mo_2O_2F_9]^-$ anion is viewed along the Mo–Mo axis) range between 9.087(21)° and 15.491(22)°. These angles are larger than those observed in $Li[Mo_2O_2F_9]$ but smaller than those observed in $K[Mo_2O_2F_9]$. A list of all torsion angles observed in $Na[Mo_2O_2F_9]$ is reported in Table S2. $Na[Mo_2O_2F_9]$ has the longest Mo–O atomic distance in the series, having a value of 1.660(5) Å. Mo–F_t atomic distances range between 1.828(4) and 1.871(4) Å. The Mo–μ-F atomic distance is 2.1489(15) Å and the Mo–μ-F–Mo angle is 150.7(3)°. A section of the crystal structure of $Na[Mo_2O_2F_9]$ is shown in Figure 4. To the best of our knowledge, the compound represents a new structure type.

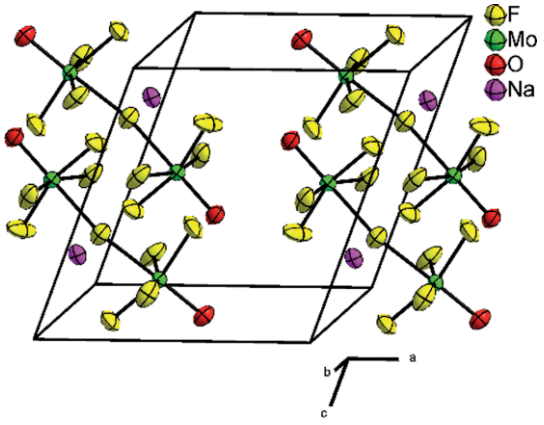

Figure 4. Section of the crystal structure of $Na[Mo_2O_2F_9]$. Displacement ellipsoids are shown at a 70 % probability level at 100 K.

3. Single Crystal Structure of $K[Mo_2O_2F_9]$

$K[Mo_2O_2F_9]$ crystallizes in the monoclinic space group $P2/c$ with the lattice parameters a = 5.4386(4), b = 5.0712(3), c = 15.1497(10) Å, β = 105.842(6)°, V = 401.96(5) Å^3, Z = 2, T = 100 K. Atomic coordinates and equivalent isotropic displacement parameters for $K[Mo_2O_2F_9]$ are reported in Table 5. It was observed that the $K[Mo_2O_2F_9]$, $Rb[Mo_2O_2F_9]$, and $Cs[Mo_2O_2F_9]$ salts are isotypic to each other, so only the potassium salt will be discussed in detail. Additionally, these salts are also isotypic to the previously reported $[H_3O]W_2O_2F_9$ salt.[23]

In the $K[Mo_2O_2F_9]$ salt, the K^+ cation is coordinated by twelve fluorine atoms, ten F_t atoms and two μ-F atoms (belonging to four different $[Mo_2O_2F_9]^-$ anions), creating a distorted anti-

Table 5. Atomic coordinates and equivalent isotropic displacement parameters U_{iso} for $K[Mo_2O_2F_9]$.

Atom	Position	x	y	z	U_{iso} /Å^2
Mo(1)	4g	0.13886(4)	0.25809(6)	0.38781(2)	0.00689(8)
F(1)	2e	0	0.1053(4)	1/4	0.0110(5)
F(2)	4g	0.3899(3)	0.3909(3)	0.33772(11)	0.0122(4)
F(3)	4g	0.6824(3)	0.0582(3)	0.59694(12)	0.0121(4)
F(4)	4g	0.1450(3)	0.0781(3)	0.09868(12)	0.0125(4)
F(5)	4g	0.0699(3)	0.5376(3)	0.16325(11)	0.0116(3)
O(1)	4g	0.2469(4)	0.3766(4)	0.49244(15)	0.0118(4)
K(1)	2f	1/2	0.82949(17)	1/4	0.01138(19)

cuboctahedral coordination polyhedron around the cation. A depiction of the coordination environment surrounding the K^+, Rb^+, and Cs^+ cations is shown in Figure S7. The coordination of the $[Mo_2O_2F_9]^-$ anions to the K, Rb, and Cs cations, respectively, leads to the formation of two-dimensional infinite sheets parallel to the *a*–*b* plane, see Figure S8.

The smallest torsion angles between adjacent F_t atoms (seen when the $[Mo_2O_2F_9]^-$ anion is viewed along the Mo–Mo axis) range between 31.596(73)° and 36.571(76)°. Similar torsion angles are observed in the rubidium salt. A complete list of torsion angles observed in the potassium, rubidium, and cesium salts is reported in Table S3. The smallest Mo–O atomic distance was observed in $K[Mo_2O_2F_9]$, having a value of 1.646(2) Å. The Mo–F_t atomic distances range between 1.8485(16) and 1.8598(17) Å, and the Mo–μ-F atomic distance is 2.1607(8) Å. The smallest Mo–μ-F–Mo angle was observed in $K[Mo_2O_2F_9]$, having a value of 137.98(11)°. When the Mo–μ-F–Mo angles in the potassium, rubidium, and cesium salts are compared, it is seen that a slight increase in the angle is observed with increase in cation size. Other than this trend, no obvious trend in Mo–μ-F–Mo angles could be determined for the $M[Mo_2O_2F_9]$ (M = Li–Cs) series. A section of the crystal structure of $K[Mo_2O_2F_9]$ is shown in Figure 5.

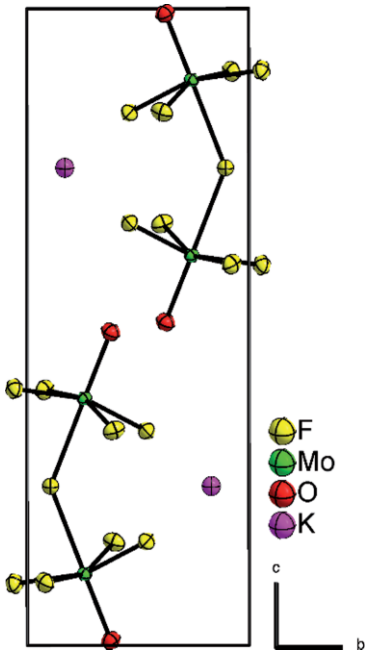

Figure 5. Section of the crystal structure of $K[Mo_2O_2F_9]$. Similar crystal structures are seen in the isotypic rubidium and cesium salts. Displacement ellipsoids are shown at a 70 % probability level at 100 K.

Furthermore, a trend among the isotypic crystal structures was observed: as the cation increases from K to Cs, the length of the *a*- and *b*-axes increase while the length of the *c*-axis decreases. The increase in cation size pushes the $[Mo_2O_2F_9]^-$ anions away from each other within the two-dimensional infinite layers. This outward displacement within the layers allows for a compression of the crystal structure along the *c*-axis as *M*···O (*M* = K–Cs) distances decrease with increases in cation size, refer to Figure S9.

4. Single Crystal Structure of $Rb[Mo_2O_2F_9]$

$Rb[Mo_2O_2F_9]$ crystallizes with the lattice parameters a = 5.6244(3), b = 5.1946(2), c = 14.9973(8) Å, β = 106.748(5)°, V = 419.58(4) Å^3, Z = 2, T = 100 K. Atomic coordinates and equivalent isotropic displacement parameters for $Rb[Mo_2O_2F_9]$ are reported in Table 6.

Table 6. Atomic coordinates and equivalent isotropic displacement parameters U_{iso} for $Rb[Mo_2O_2F_9]$.

Atom	Position	x	y	z	U_{iso} /Å^2
Mo(1)	4g	0.14072(3)	0.25197(3)	0.39040(2)	0.01186(8)
F(1)	2e	0	0.1058(4)	1/4	0.0157(3)
F(2)	4g	0.3870(2)	0.3734(3)	0.34041(10)	0.0181(3)
F(3)	4g	0.6941(2)	0.0620(3)	0.59307(10)	0.0170(3)
F(4)	4g	0.1388(2)	0.0847(3)	0.09652(10)	0.0175(3)
F(5)	4g	0.0578(3)	0.5299(3)	0.16186(10)	0.0174(3)
O(1)	4g	0.2504(3)	0.3680(3)	0.49696(12)	0.0183(3)
Rb(1)	2f	1/2	0.82533(6)	1/4	0.01476(9)

The torsion angles between adjacent F_t atoms (Figure S4) are similar to those in $K[Mo_2O_2F_9]$, and range between 35.034(62)° and 39.652(66)°. The Mo–O atomic distance in $Rb[Mo_2O_2F_9]$ is 1.6522(17) Å, while the Mo–F_t atomic distances range between 1.8547(14) and 1.8649(14) Å. The longest Mo–μ-F atomic distance in the series was observed in the rubidium salt, having a value of 2.1624(7) Å. $Rb[Mo_2O_2F_9]$ has a Mo–μ-F–Mo angle of 138.89(10)°, a value larger than that observed in the potassium salt, but smaller than that observed in the cesium salt.

5. Single Crystal Structure of $Cs[Mo_2O_2F_9]$

$Cs[Mo_2O_2F_9]$ crystallizes with the lattice parameters a = 5.9162(3), b = 5.4203(3), c = 14.7154(7) Å, β = 108.554(4)°, V = 447.36(4) Å^3, Z = 2, T = 100 K. Atomic coordinates and equivalent isotropic displacement parameters for $Cs[Mo_2O_2F_9]$ are reported in Table 7.

Table 7. Atomic coordinates and equivalent isotropic displacement parameters U_{iso} for $Cs[Mo_2O_2F_9]$.

Atom	Position	x	y	z	U_{iso} /Å^2
Mo(1)	4g	0.14438(7)	0.24268(7)	0.39465(3)	0.01325(8)
F(1)	2e	0	0.1092(7)	1/4	0.0173(7)
F(2)	4g	0.3826(5)	0.3487(6)	0.3464(2)	0.0206(5)
F(3)	4g	0.7112(5)	0.0652(5)	0.5882(2)	0.0186(5)
F(4)	4g	0.1288(5)	0.0977(6)	0.0950(2)	0.0197(5)
F(5)	4g	0.0341(5)	0.5174(5)	0.1586(2)	0.0211(6)
O(1)	4g	0.2579(6)	0.3483(7)	0.5051(2)	0.0212(7)
Cs(1)	2f	1/2	0.80649(7)	1/4	0.01527(9)

The torsion angles between adjacent F_t atoms (Figure S4) range between 40.607(13)° to 44.819(14)°. The Mo–O atomic

distance in $Cs[Mo_2O_2F_9]$ is 1.651(3) Å. The Mo–F_t atomic distances range between 1.847(3) and 1.860(3) Å, and the Mo–μ-F atomic distance is 2.1509(14) Å. The Mo–$F_μ$–Mo angle has a value of 140.7(2)°, giving rise to an angle larger than those observed in the potassium and rubidium salts, but smaller than those found in the sodium and lithium salts.

Upon comparison of the salts reported here, it is seen that $Li[Mo_2O_2F_9]$ crystallizes in the triclinic space group $P\bar{1}$, whereas the remaining salts crystallize in the monoclinic space group *P*2/*c*. The potassium, rubidium, and cesium salts were observed to be isotypic to one another, as well as the previously reported $H_3O[W_2O_2F_9]$ salt. In the crystal structures of the $M[Mo_2O_2F_9]$ (*M* = Li–Cs) salts, the $[Mo_2O_2F_9]^-$ anion coordinates to the respective cation to form infinite sheets. These sheets are parallel to the (011) plane in $Li[Mo_2O_2F_9]$, the *b*–*c* plane in $Na[Mo_2O_2F_9]$, and the *a*–*b* plane in the potassium, rubidium and cesium salts.

The Mo–μ-F, Mo–F_t, and Mo–O atomic distances found in the $M[Mo_2O_2F_9]$ (*M* = Li–Cs) salts are comparable to those found in other molybdenum fluorides and oxyfluorides.[11,27] No obvious explanation could be found to explain the trend in Mo–μ-F–Mo angles observed in the salts reported here. It was observed that torsion angles between adjacent F_t atoms, however, steadily increased with increasing cation size.

Lastly, to concluded this section, a comparison of the Mo^{VI} salts reported in this work will be made to the previously reported $K_2(NMe_4)[Mo^V_2O_2F_9]\cdot H_2O$ and $(NH_4)_3[Mo^V_2O_2F_9]$ salts. In all salts, an $[Mo_2O_2F_9]$ anion is present, the charge of which is dictated by oxidation states of the molybdenum atoms. The most noticeable difference between the $[Mo^{VI}_2O_2F_9]^-$ anions and the previously reported $[Mo^V_2O_2F_9]^{3-}$ anions are the values of the Mo–μ-F–Mo angles. In the salts reported here, the Mo–$F_μ$–Mo angles range from 137.98(11)° to 158.89(12)°. These angles are much larger in the previously reported Mo^{+V} salts, having values of 169.4(3)° for $K_2(NMe_4)[Mo^V_2O_2F_9]\cdot H_2O$ and 180.0° for $(NH_4)_3[Mo^{(V)}_2O_2F_9]$. This observation is expected since the repulsion arising from the additional negative charge found in the $[Mo^{(V)}_2O_2F_9]^{3-}$ salts can be mitigated by larger Mo–$F_μ$–Mo angles. Furthermore, upon comparison of atomic distances in the $[Mo^V_2O_2F_9]^{3-}$ anions to the $[Mo^{VI}_2O_2F_9]$ anions reported here, it was shown that the Mo–O distances are comparable, whereas the Mo–F atomic distances are, on average, longer in the $[Mo^V_2O_2F_9]^{3-}$ anions. Again, such an observation is expected because the presence of additional negative charge on the $[Mo^V_2O_2F_9]^{3-}$ anion leads to increased electronic repulsion between the F and Mo atoms, which subsequently increases Mo–F atomic distances.

Infrared Spectroscopy

An IR spectrum for each $M[Mo_2O_2F_9]$ (*M* = Li–Cs) salt was collected at 25 °C in the region of 4000 to 400 cm^{-1}. Band positions are listed in Table 8. Calculated IR spectra were obtained for the solid-state structure of each salt using the DFT-PBE0 density functional method; combination bands and overtones

Table 8. Experimental IR bands observed in the $M[Mo_2O_2F_9]$ (*M* = Li–Cs) salts. When given, a description of vibrational modes is as follows: ν = stretching, s = symmetric, as = asymmetric. $F_μ$ refers to bridging fluorine atoms while F_t refers to terminal fluorine atoms. All band locations are given in cm^{-1}.

$Li[Mo_2O_2F_9]$	$Na[Mo_2O_2F_9]$	$K[Mo_2O_2F_9]$	$Rb[Mo_2O_2F_9]$	$Cs[Mo_2O_2F_9]$
403 ν(Mo–F_t) 470 ν(Mo–F_t)	434 ν(Mo–F_t)	412 ν(Mo–$F_μ$) 451	407 ν(Mo–$F_μ$) 468	408 ν(Mo–$F_μ$) 451 492
552 $ν_{as}$(Mo–F_t)	564 $ν_{as}$(Mo–F_t)	569 $ν_{as}$(Mo–F_t)	553 ν(Mo–F_t)	593 ν(Mo–F_t)
614 $ν_s$(Mo–F_t) 663 $ν_s$(Mo–F_t) 697 ν(Mo–$F_μ$; Mo–F_t)	630 ν(Mo–$F_μ$; Mo–F_t)	625 $ν_s$(Mo–F_t)	627 $ν_s$(Mo–F_t) 649 $ν_s$(Mo–F_t)	646 $ν_s$(Mo–F_t)
847	846	863	857	850
958 988	941 976	911	907 956 977	968
1017 ν(Mo–O)	1019 ν(Mo–O)	1015 ν(Mo–O) 1037 ν(Mo–O)	1018 ν(Mo–O) 1034 ν(Mo–O)	1016 ν(Mo–O)
1168 ($ν_2$ HF_2^-)[30]		1101 ($ν_2$ $H_2F_3^-$)[30] 1157 ($ν_2$ $H_2F_3^-$)[31]		
	1211 ($ν_2$ HF_2^-)[29,30]			
		1300 1366		
	1580 ($ν_3$ HF_2^-)[29,30]			
1720 ($ν_3$ HF_2^-)[30]		1743 ($ν_3$ $H_2F_3^-$)[30,31]		
		2359 (combination $H_2F_3^-$)[31]		

bands were not accounted for. Experimental spectra correlated well with the calculated spectra (Figure 6; Figures S10–S13, Tables S4–S8), however, the experimentally obtained spectra show additional bands belonging to by-products. Powder diffraction patterns of each sample were recorded to aid in the identification of the by-products. However, due to the quality of the diffraction patterns, unambiguous identification of the by-products was not possible. Therefore, a discussion of potential by-products will be provided based on the reported IR spectra. Powder diffraction patterns are shown in Figures S15–S19.

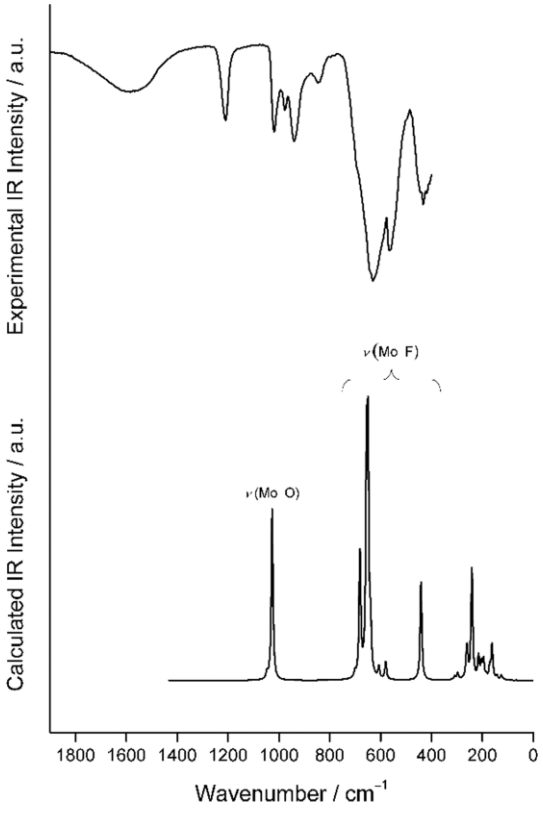

Figure 6. Experimentally obtained (above) and calculated (below) IR spectrum of $Na[Mo_2O_2F_9]$.

Band assignments in Table 8, when given, were made by the visual inspection of the calculated normal modes using the J mol software[28] and through direct comparison to the experimentally obtained bands. In each spectrum, no bands were observed beyond 2500 cm^{-1}. As an example of an IR spectrum typical of this series of salts, the IR spectrum of $Na[Mo_2O_2F_9]$, in the region of 2500 cm^{-1} to 400 cm^{-1}, is shown in Figure 6. The remaining experimentally obtained and calculated IR spectra are shown in Figures S10–S13. The IR spectrum of each salt is dominated by Mo–F stretching in the region of about 400 cm^{-1} to 700 cm^{-1}, along with a prominent Mo–O stretching band seen around 1015 cm^{-1}.

In the IR spectra of $Li[Mo_2O_2F_9]$ and $Na[Mo_2O_2F_9]$, the deformation vibration ν_2 and the antisymmetric stretching vibration ν_3 of the bifluoride ion, HF_2^-, are clearly visible (refer to Table 8).[29,30] The presence of bifluoride and other $[F(HF)_n]^-$ (n = typically 2 to 4) impurities likely arise from the fact that the alkali metal fluorides were present in excess in the reaction mixtures. The IR spectrum of $K[Mo_2O_2F_9]$ (Figure S11) shows bands at 451, 1015, 1037, 1101, 1157, 1743 and 2359 cm^{-1}. Previous studies report the IR bands of KF•2HF to occur at 480 (ν_1), 1030–1150 (ν_2), 1780 (ν_3) 2000, and 2350 cm^{-1}.[30,31] The presence of similar bands in the spectrum of $K[Mo_2O_2F_9]$ may arise from the presence of KF•2HF in the product mixture. However, since the Mo–O stretching bands in the $[Mo_2O_2F_9]^-$ anion occur in the region of 1000–1100 cm^{-1}, the bands arising from any KF•2HF would be overlapped with these bands. This makes the detection of any possible KF•2HF present difficult since its band intensities cannot be adequately measured in this region. Given the reaction conditions, however, it should be possible to observe the presence of fluorides such as KF•2HF. Moreover, the spectrum of $K[Mo_2O_2F_9]$ shows bands at 1300, and 1366 cm^{-1}. These two bands may also arise from higher HF adducts of potassium fluoride, however, direct assignment of these bands to a particular fluoride could not be made. The IR spectra of $Rb[Mo_2O_2F_9]$ and $Cs[Mo_2O_2F_9]$ showed no evidence of bifluoride or higher HF adduct formation.

The spectra of all $M[Mo_2O_2F_9]$ (M = Li–Cs) salts show bands in the region of about 850 to 990 cm^{-1} which do not belong to the $[Mo_2O_2F_9]^-$ anion. In the work of Beuter and Sawodny, in which $Rb[Mo_2O_2F_9]$ was reported, they observed a series of bands in the IR region of 930 to 975 cm^{-1}.[16] They attributed the observation of these bands to hydrolysis products of the $Rb[Mo_2O_2F_9]$ salt.[16] However, since the samples presented in this work were handled under strictly-dried atmospheres, and because there is no evidence of water or hydroxides in the spectra presented here, it seems highly unlikely that the bands observed in this work arise because of hydrolysis products. Moreover, in the work of Bougon and co-workers, $NO[Mo_2O_2F_9]$ and $ClOF_2[Mo_2O_2F_9]$ were synthesized and characterized through IR spectroscopy. The bands arising from the $[Mo_2O_2F_9]^-$ anion in the $NO[Mo_2O_2F_9]$ and $ClOF_2[Mo_2O_2F_9]$ salts correlate well to those observed in this work. However, the authors observed bands at 910, 935, 967, 973, and 983 cm^{-1} in the spectrum of $NO[Mo_2O_2F_9]$ which do not belong to the $[Mo_2O_2F_9]^-$ anion. They assigned the band at 983 cm^{-1} to $NO[MoOF_5]$ but gave no further discussion on the occurrence of the remaining bands.[12]

To determine if the $[MoOF_5]^-$ anion is responsible for the observation of bands arising between 850 and 990 cm^{-1} in the spectra reported here, an IR spectrum of a C_{4v} $[MoOF_5]^-$ anion was calculated using the DFT-PBE0 density functional method and the def2-TZVP basis set (Figure S19, Table S9). The calculated spectrum shows a band at 1037 cm^{-1}, correlating to Mo–O stretching and bands below 700 cm^{-1} correlating to Mo–F stretching (and other vibrational modes), but does not show any bands in the region of about 700 to 1000 cm^{-1}. This calculated IR spectrum correlates well to previously reported IR spectra of salts containing the $[MoOF_5]^-$ anion.[12,32] Moreover, the calculated IR spectrum of the $[MoOF_5]^-$ anion is quite similar to the calculated IR spectra of the $[Mo_2O_2F_9]^-$ anion. Therefore, it would be hard to determine the presence of the $[MoOF_5]^-$ anion in the sample mixtures with IR spectroscopy alone since any bands arising from this anion would likely overlap with those arising from the $[Mo_2O_2F_9]^-$ anion. Based on the calcu-

lated IR spectrum, though, it can be said that the bands arising between 850 to 970 cm^{-1} in the spectra reported in this work are not observed because of a possible presence of the $[MoOF_5]^-$ anion. The fact that similar bands are seen in the IR spectra of previously reported $[Mo_2O_2F_9]^-$ anions, though, may provide insight into the complex equilibria that seemingly exists during the formation of the $[Mo_2O_2F_9]^-$ anion.

Raman Spectroscopy

Raman spectra were obtained for each $M[Mo_2O_2F_9]$ (M = Li–Cs) salt at 25 °C from about 0 to 1200 cm^{-1}. Except for $K[Mo_2O_2F_9]$, all spectra were recorded at an excitation wavelength of 532 nm. The $K[Mo_2O_2F_9]$ salt showed strong fluorescence at this wavelength and so Raman data for this salt was collected at an excitation wavelength of 785 nm. Band locations for these experimental spectra are listed in Table 9. Calculated Raman spectra from 0 to 1200 cm^{-1} were obtained for the solid-state structures of each salt using the DFT-PBE0 density functional method. Experimentally obtained spectra correlated well with the calculated spectra, however, the experimentally obtained spectra show additional bands belonging to by-products (Figure 7; Figures S20–S23, Tables S10–S14). Powder diffraction patterns of each sample were recorded to aid in the identification of the by-products. However, due to the quality of the diffraction patterns, unambiguous identification of the by-products was not possible. Therefore, a discussion of potential by-products will be provided based on the reported Raman spectra.

Band assignments in Table 9, when given, were made by the visual inspection of the calculated normal modes using the J mol software[28] and through direct comparison to the experimentally obtained bands. As an example of a typical spectrum obtained from these salts, the Raman spectrum of $Na[Mo_2O_2F_9]$ is given in Figure 7. The remaining experimentally obtained and calculated Raman spectra are shown in Figures S20–S24.

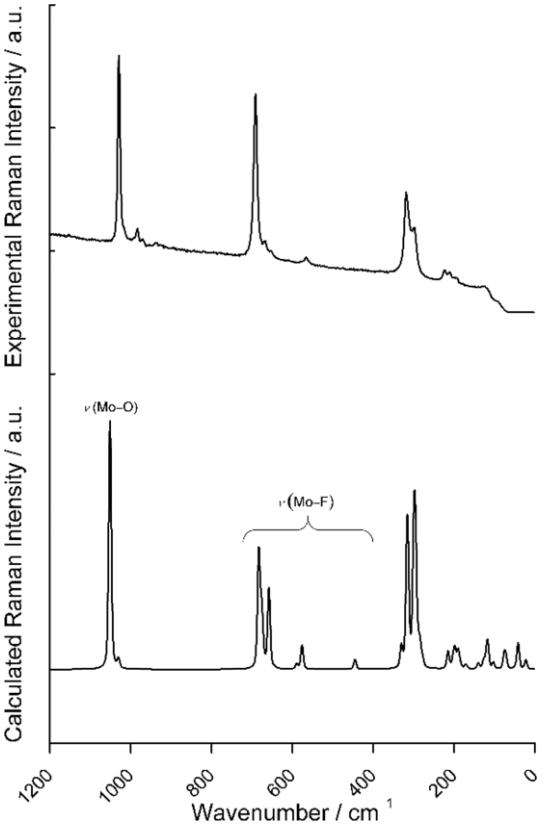

Figure 7. Experimentally obtained (above) and calculated (below) Raman spectrum of $Na[Mo_2O_2F_9]$.

Table 9. Experimental Raman bands observed in the $M[Mo_2O_2F_9]$ (M = Li–Cs) salts. When given, a description of vibrational modes is as follows: ν = stretching, δ = deformation, ρ_w = wagging, ρ_r = rocking, ρ_t = twisting, s = symmetric, as = asymmetric. F_μ refers to the bridging fluorine atoms and F_t refers to terminal fluorine atoms.

$Li[Mo_2O_2F_9]$	$Na[Mo_2O_2F_9]$	$K[Mo_2O_2F_9]$[a]	$Rb[Mo_2O_2F_9]$	$Cs[Mo_2O_2F_9]$
	194 $\rho_t(F_t–Mo–F_t)$		197 $\rho_t(F_t–Mo–F_t)$	192 $\rho_t(F_t–Mo–F_t)$
216 $\rho_r(F_t–Mo–F_t)$	211 $\delta(F_t–Mo–F_t)$ 223 $\delta(F_t–Mo–Ft)$ 299 $\delta(F_t–Mo–O)$	202 $\rho_t(F_t–Mo–F_t)$ 220 $\delta(F_t–Mo–F_t)$; $\rho_r(F_t–Mo–F_t)$	221 $\delta(F_t–Mo–F_t)$; $\rho_t(F_t–Mo–F_t)$ 268 $\delta(F_\mu–Mo–O)$	220 $\delta(F_t–Mo–F_t)$; $\rho_r(F_t–Mo–F_t)$ 268 $\delta(F_\mu–Mo–O)$
304 $\delta(F_t–Mo–O)$ 319 $\delta(F_t–Mo–O)$	318 $\delta(F_t–Mo–O)$	305 $\delta(F_t–Mo–F_t)$; $\rho_w(F_t–Mo–F_t)$ 313 $\delta(F_t–Mo–F_t$; $F_t–Mo–O)$ 319 $\rho_r(F_\mu–Mo–O)$	303 $\delta(F_t–Mo–F_t)$; $\rho_t(F_t–Mo–O)$ 317 $\delta(F_t–Mo–O)$ 396	
416				404 $\nu(Mo–F_\mu)$
	566 $\nu_{as}(Mo–F_t)$	571 $\nu_{as}(Mo–F_t)$	572 $\nu_{as}(Mo–F_t)$	558 576 $\nu_{as}(Mo–F_t)$
669 $\nu_s(Mo–F_t)$ 694 $\nu(Mo–F_\mu)$	668 $\nu(Mo–F_t)$ 691 $\nu_s(Mo–F_t)$	646 $\nu_s(Mo–F_t)$ 681 $\nu(Mo–F_t)$	656 $\nu_s(Mo–F_t)$; $\nu_{as}(Mo–F_t)$ 678 $\nu_s(Mo–F_t)$	676 $\nu_s(Mo–F_t)$
941 988	938 971 983		922 962 977	914 954 976
1027 ν(Mo–O)	1029 ν(Mo–O)	1028 ν(Mo–O)	1025 ν(Mo–O)	1020 ν(Mo–O)

[a] Data collected at a wavelength of 785 nm.

The bands arising from the $[Mo_2O_2F_9]^-$ anion in the $M[Mo_2O_2F_9]$ (M = Li–Cs) salts correlate well with the Raman bands reported for the $ClOF_2[Mo_2O_2F_9]$ and $NO[Mo_2O_2F_9]$ salts.[12] The Raman spectra of each salt, in the region of about 0 to 400 cm^{-1}, is dominated by various Mo–O and Mo–F deformation, wagging, rocking, and twisting modes. Similar to the IR spectra, the Raman spectra show bands in the 400 to 700 cm^{-1} region, arising from Mo–F stretching modes and the Mo–O stretching modes were observed around 1020 cm^{-1}.

In the IR spectra of $Li[Mo_2O_2F_9]$ and $Na[Mo_2O_2F_9]$, the presence of the HF_2^- anion is clearly visible (Figure 7; Figure S20). However, evidence for the presence of the bifluoride anion in the Raman spectra is not as obvious. The bifluoride anion has two reported Raman active modes: the F–H–F$^-$ symmetric stretching mode $\nu_1(A_{1g})$ and the librational lattice mode (E_g), which occur at about 630 and 145 cm^{-1}, respectively.[33] Since the backgrounds in the early region of the Raman spectra are large, it is hard to determine if any bands are present around 145 cm^{-1}. Additionally, bands arising from the Mo–F stretching modes of the $[Mo_2O_2F_9]^-$ anion occur in the region where the symmetric stretching mode of the HF_2^- anion is expected to occur. It is, therefore, difficult to identify the presence of the bifluoride anion in these Raman spectra. Moreover, the presence of the $H_2F_3^-$ anion was evidenced in the IR spectrum of $K[Mo_2O_2F_9]$. However, the Raman spectrum of $K[Mo_2O_2F_9]$ shows no foreign bands (i.e. all bands could be assigned to the $[Mo_2O_2F_9]^-$ anion). Reasons for this observation may stem from the fact that this Raman spectrum was collected at 785 nm and it was noticed that the background in this spectrum was much higher than those seen in the other spectra. It could be that the noise in this spectrum masks any bands arising from the $H_2F_3^-$ anion.

Just as in the IR spectra, the Raman spectra of all salts, with the exception of $K[Mo_2O_2F_9]$, show a series of bands around 900 to 1000 cm^{-1} which are not explained by the presence of the $[Mo_2O_2F_9]^-$ anion. In the spectra of $Li[Mo_2O_2F_9]$, $Rb[Mo_2O_2F_9]$, and $Cs[Mo_2O_2F_9]$, these bands have considerable intensities when compared to the bands arising from the $[Mo_2O_2F_9]^-$ anion. In the spectrum of $Na[Mo_2O_2F_9]$, however, these bands are quite weak in comparison to the $[Mo_2O_2F_9]^-$ anion bands, and in the spectrum of $K[Mo_2O_2F_9]$ these bands are missing entirely. In the work of Bougon and co-workers, in which $NO[Mo_2O_2F_9]$ was synthesized, they described an IR band at 983 cm^{-1}, which was sometimes present in the Raman spectrum as a weak band.[12] They attribute this band to the presence of $NO[MoOF_5]$.

Again, to determine if the $[MoOF_5]^-$ anion was present in our samples, a Raman spectrum of a C_{4v} $[MoOF_5]^-$ anion was calculated using the DFT-PBE0 density functional method and the def2-TZVP basis set and is shown in Figure S24 (band locations and intensities reported in Table S15). This spectrum showed a band at 1038 cm^{-1} corresponding to Mo–O stretching and several other bands below 700 cm^{-1} corresponding to Mo–F stretching (and other vibrational modes). This calculated Raman spectrum correlates well to previously reported Raman spectra of salts containing the $[MoOF_5]^-$ anion.[12,32] Moreover, the calculated Raman spectrum of the $[MoOF_5]^-$ anion is somewhat similar to the calculated Raman spectra of the $[Mo_2O_2F_9]^-$ anions calculated here. Therefore, as was the conclusion in the IR spectroscopy analysis, it would be hard to determine the presence of the $[MoOF_5]^-$ anion in the sample mixtures with Raman spectroscopy alone. Based on the calculated Raman spectrum, though, it can be said that the bands arising between 900 to 970 cm^{-1} in the Raman spectra reported in this work are not observed because of a possible presence of the $[MoOF_5]^-$ anion.

Conclusions

A series of $M[Mo_2O_2F_9]$ (M = Li–Cs) salts was synthesized through the reaction of $MoOF_4$ with the respective alkali metal fluoride in an aHF solution. The crystal structures of these salts were studied using single-crystal X-ray diffraction. All crystal structures show a layer structure motif. The potassium, rubidium and cesium salts are isotypic. In the case of the lithium salt, disorder was shown by one of the lithium atoms. In all compounds, the $[Mo_2O_2F_9]^-$ anion is observed, which can be thought of as two $MoOF_4$ units bridged by a fluorine anion. IR and Raman spectroscopy were employed to obtain the vibrational spectra of the $M[Mo_2O_2F_9]$ (M = Li–Cs) salts. Calculated IR and Raman spectra were obtained for the solid state of each salt using the DFT-PBE0 density functional method in order to aid in the assignment of bands in the experimentally obtained spectra. The calculated IR and Raman spectra agree nicely with the experimentally obtained spectra. Evidence for hydrogen fluoride adducts, such as $[F(HF)_n]^-$ (n = 1,2) were observed in some cases. The synthesis of phase-pure $M[Mo_2O_2F_9]$ (M = Li–Cs) salts was not realized, although their phase-pure synthesis may be possible in solvents which would not directly interact with the starting materials.

It is clear that the reaction conditions leading to the production of the $M[Mo_2O_2F_9]$ (M = Li–Cs) salts is quite complex, as indicated by the variety of by-products observed within the samples (as evidenced by the IR and Raman spectra and powder X-ray diffraction patterns). Studies in the past which have tried to produce the $[MoOF_5]^-$ anion have observed that, in systems with relatively low free F$^-$ concentration, the $[Mo_2O_2F_9]^-$ anion is preferably produced. If the concentration of free F$^-$ is increased, by increasing the concentration of the fluoride salt(s) used, then the $[MoOF_5]^-$ anion and, subsequently, the $[MoOF_6]^{2-}$ anion may be successfully produced. Since the $M[Mo_2O_2F_9]$ (M = Li–Cs) salts produced in this work were synthesized using a 1:1 molar ratio of $MoOF_4$ to MF (M = Li–Cs), which gave moderate concentrations of free F$^-$ in aHF solution, it is understandable that the $M[Mo_2O_2F_9]$ (M = Li–Cs) salts were preferably obtained over species such as $M[MoOF_5]$ or $M_2[MoOF_6]$ (M = Li–Cs). The $M[MoOF_5]$ and $M_2[MoOF_6]$ (M = Li–Cs) salts may be obtainable if the starting concentration of the respective alkali metal fluoride is increased substantially in comparison to $MoOF_4$.

Experimental Section

General Procedures and Materials: All operations were performed in either stainless steel (316 L) or Monel metal vacuum lines, which

were passivated with 100 % fluorine at various pressures before use. Preparations were carried out in an atmosphere of dry and purified Argon (5.0, Praxair). Molybdenum hexafluoride (99 %, ABCR) was distilled once prior to usage. Anhydrous HF (Fluka Analytical, > 99.9 %), which was stored over $K_2[NiF_6]$, was distilled twice before use. Fluorinated ethylene propylene, FEP (15.90x19.05 mm – 3/4"), was used to produce reaction vessels.

Synthesis of $M[Mo_2O_2F_9]$ (M = Li–Cs): First, $MoOF_4$ was synthesized through the hydrolysis of MoF_6 in aHF using quartz wool. For this reaction, 0.56 grams of quartz wool, SiO_2, (9.32 mmol) was added to an FEP vessel and attached to a metal vacuum line and evacuated and flushed with argon three times. 3 mL of aHF and 5 grams of MoF_6 (23.82 mmol) were condensed onto the quartz wool at –196 °C. The reaction vessel was warmed to room temperature and stored for 1 week. After the reaction was completed, as indicated by complete solvation of the SiO_2 wool, all volatile products were removed and the $MoOF_4$ was stored under argon in a glovebox. IR and powder X-ray diffraction showed no evidence of impurities in the $MoOF_4$ sample.

To produce the $M[Mo_2O_2F_9]$ (M = Li–Cs) salts, an approximately 1:1 molar ratio of $MoOF_4$ and MF (M = Li–Cs) was mixed using an agate mortar and pestle in an inert atmosphere glovebox and transferred to an FEP reaction vessel. The reaction vessel was attached to a metal vacuum line and evacuated and flushed with argon 3 times. 4 to 6 mL of aHF was condensed onto the reactants at –196 °C. The reaction vessels were warmed to room temperature, producing colorless solutions in all cases. Once all reactants had dissolved, the aHF was slowly pumped off to produce colorless, crystalline samples. The products were transferred to an inert atmosphere glovebox for storage. It was noticed after months of storage the samples began to turn gray-blue.

Synthesis of $Li[Mo_2O_2F_9]$: Under inert atmosphere, 123.91 mg of $MoOF_4$ (0.66 mmol) and 17.90 mg of LiF (0.69 mmol) were placed in an FEP reaction vessel. 4 mL of aHF were condensed on top of the reaction mixture. After warming to room-temperature the aHF was slowly pumped off over a period of 5 hours. Product was stored in a PTFE container under argon in a glovebox.

Synthesis of $Na[Mo_2O_2F_9]$: Under inert atmosphere, 125.07 mg of $MoOF_4$ (0.67 mmol) and 27.90 mg of NaF (0.66 mmol) were placed in an FEP reaction vessel. 4 mL of aHF were condensed on top of the reaction mixture. After warming to room-temperature the aHF was slowly pumped off over a period of 5 hours. Product was stored in a PTFE container under argon in a glovebox.

Synthesis of $K[Mo_2O_2F_9]$: Under inert atmosphere, 126.15 mg of $MoOF_4$ (0.67 mmol) and 39.08 mg of KF (0.67 mmol) were placed in an FEP reaction vessel. 4 mL of aHF were condensed on top of the reaction mixture. After warming to room-temperature the aHF was slowly pumped off over a period of 5 hours. Product was stored in a PTFE container under argon in a glovebox.

Synthesis of $Rb[Mo_2O_2F_9]$: Under inert atmosphere, 127.82 mg of $MoOF_4$ (0.68 mmol) and 69.91 mg of RbF (0.67 mmol) were placed in an FEP reaction vessel. 6 mL of aHF were condensed on top of the reaction mixture. After warming to room-temperature the aHF was slowly pumped off over a period of 5 hours. Product was stored in a PTFE container under argon in a glovebox.

Synthesis of $Cs[Mo_2O_2F_9]$: Under inert atmosphere, 128.78 mg of $MoOF_4$ (0.69 mmol) and 102.82 mg of CsF (0.68 mmol) were placed in an FEP reaction vessel. 6 mL of aHF were condensed on top of the reaction mixture. After warming to room-temperature the aHF was slowly pumped off over a period of 5 hours. Product was stored in a PTFE container under argon in a glovebox.

Single-Crystal X-ray Diffraction: X-ray structure analysis of the single crystals of $M[Mo_2O_2F_9]$ (M = Li–Cs) were carried out with a STOE IPDS 2T diffractometer with plane graphite-monochromated molybdenum radiation (Mo-K_α, λ = 0.71073 Å) generated by a sealed X-ray tube (12 × 0.4 mm long fine focus), and a detector resolution of 6.67 pixels mm^{-1}. Evaluation and integration of the diffraction data was carried out using the X-Area software, and absorption corrections were made through integration using the X-Red32 and X-Shape program within the parent software.[34] The structures were solved using Direct Methods (SHELXT 2014/5) and refined against F^2 (SHELXL-2018/3).[35,36] Representations of the crystal structure were created using the Diamond software.[37]

Further details of the crystal structure investigation(s) may be obtained from Fachinformationszentrum Karlsruhe, 76344 Eggenstein-Leopoldshafen, Germany (fax: +49-7247-808-666; e-mail: crysdata@fiz-karlsruhe.de), on quoting the depository numbers CSD-1903263 ($Li[Mo_2O_2F_9]$), CSD-1903264 ($Na[Mo_2O_2F_9]$), CSD-1903262 ($K[Mo_2O_2F_9]$), CSD-1903266 ($Rb[Mo_2O_2F_9]$), and CSD-1903265 ($Cs[Mo_2O_2F_9]$).

Powder X-ray Diffraction: Powder X-ray diffraction patterns were obtained with a StadiMP diffractometer (Stoe) using Cu-K_α radiation (λ = 1.54059 Å), a germanium monochromator and a Mythen1K detector. The samples were placed in 0.3 mm glass capillaries and sealed using a hot tungsten wire and Pizein. The data were processed in and graphical representations were created using the WinXPOW software.[38]

IR Spectroscopy: The IR spectra were measured on an alpha FTIR spectrometer (Bruker) using a diamond ATR unit under an Ar atmosphere. The spectrum was processed with the OPUS software package.[39]

Raman Spectroscopy: The $M[Mo_2O_2F_9]$ (M = Li–Cs) salts were loaded into 0.3 mm borosilicate capillaries and the Raman spectra were measured in backscattering geometry by means of a Raman microscope inVia (Renishaw), using a frequency-doubled Nd:YAG laser (532 nm wavelength). The spectra were recorded in confocal mode between 2 cm^{-1} and 1792 cm^{-1}. The laser power was reduced to 5 % to prevent degradation of the samples.

Computational Details: Periodic quantum chemical calculations were carried out for the $M[Mo_2O_2F_9]$ (M = Li–Cs) salts using the DFT-PBE0 density functional method (DFT).[40,41] A triple-zeta-valence + polarization (TZVP) level basis set was applied for Mo and split-valence + polarization (SVP) level basis sets were applied for the other atoms. The basis set for Mo was taken from a previous study on MoF_5.[27] The basis sets for Li, Na, K, Rb, Cs, O, and F were also taken from previous studies (see Supporting Information for full basis set details).[42–45] All calculations were carried out using the CRYSTAL17 program package.[46] The reciprocal space for the salts was sampled using the respective Monkhorst–Pack-type k-point grid: $Li[Mo_2O_2F_9]$: 4x3x2, $Na[Mo_2O_2F_9]$: 3x4x3, $K[Mo_2O_2F_9]$: 4x4x2, $Rb[Mo_2O_2F_9]$: 4x4x2, $Cs[Mo_2O_2F_9]$: 2x4x2. For the evaluation of the Coulomb and exchange integrals (TOLINTEG), tight tolerance factors of 8, 8, 8, 8, and 16 were used for all calculations. Both the atomic positions and lattice constants were fully optimized within the constraints imposed by the space group symmetry. Default optimization convergence thresholds were applied in all calculations. The XYZ coordinates used in the computational calculations of each salt in the solid-state, and the $[MoOF_5]^-$ anion, are reported in Tables S16–S21.

The harmonic vibrational frequencies, IR intensities, and Raman intensities were obtained by using the computational scheme implemented in CRYSTAL17 [5–8].[47–50] The Raman intensities were calcu-

lated for a polycrystalline powder sample (total isotropic intensity in arbitrary units). The Raman spectra were obtained by using a pseudo-Voigt band profile (50:50 Lorentzian:Gaussian) and an FWHM of 8 cm^{-1}. The Raman spectra were simulated taking into account the experimental setup (T = 298.15 K, λ = 532 nm). For the IR spectra, a Lorentzian lineshape and an FWHM of 8 cm^{-1} was used. The band assignments were carried out by visual inspection of the normal modes using the J mol program package.[28]

Acknowledgments

F. K. would like to thank the Deutsche Forschungsgemeinschaft (DFG) for funding and Solvay for their donations of fluorine. A. J. K. thanks CSC, the Finnish IT Center for Science, for computational resources. The authors would also like to thank Prof. Dr. Bernhard Roling for Raman spectroscopy measurement time.

Keywords: Molybdenum · Fluorides · Oxides · Crystal structures · IR spectroscopy · Raman spectroscopy

[1] J. Ravez, G. Peraudeau, H. Arend, S. C. Abrahams, P. Hagenmüller, *Ferroelectrics* **1980**, *26*, 767–769.
[2] Z. G. Ye, J. Ravez, J.-P. Rivera, J.-P. Chaminade, H. Schmid, *Ferroelectrics* **1991**, *124*, 281–286.
[3] R. A. Wheeler, M. H. Whangbo, T. Hughbanks, R. Hoffmann, J. K. Burdett, T. A. Albright, *J. Am. Chem. Soc.* **1986**, *108*, 2222–2236.
[4] A. K. Stover, J. R. Gutnick, A. N. Sarjeant, A. J. Norquist, *Inorg. Chem.* **2007**, *46*, 4389–4391.
[5] D. W. Aldous, P. Lightfoot, *J. Fluorine Chem.* **2012**, *144*, 108–113.
[6] R. Mattes, K. Mennemann, N. Jäckel, H. Rieskamp, H.-J. Brockmeyer, *J. Less-Common Met.* **1980**, *76*, 199–212.
[7] H. Lin, B. Yan, P. D. Boyle, P. A. Maggard, *J. Solid State Chem.* **2006**, *179*, 217–225.
[8] J. L. Fourquet, H. Duroy, M. P. Crosnier-Lopez, *Z. Anorg. Allg. Chem.* **1997**, *623*, 439–443.
[9] O. Ruff, F. Eisner, *Ber. Dtsch. Chem. Ges.* **1907**, *40*, 2926–2935.
[10] A. J. Edwards, G. R. Jones, *J. Chem. Soc. A* **1969**, 1651.
[11] A. J. Edwards, B. R. Steventon, *J. Chem. Soc. A* **1968**, 2503.
[12] R. Bougon, T. Bui Huy, P. Charpin, *Inorg. Chem.* **1975**, *14*, 1822–1830.
[13] J. H. Holloway, G. J. Schrobilgen, *Inorg. Chem.* **1980**, *19*, 2632–2640.
[14] Yu. A. Buslaev, Yu. V. Kokunov, V. A. Bochkareva, E. M. Shustorovich, *J. Struct. Chem.* **1972**, *13*, 491–492.
[15] J. H. Holloway, G. J. Schrobilgen, *Inorg. Chem.* **1981**, *20*, 3363–3368.
[16] A. Beuter, W. Sawodny, *Angew. Chem. Int. Ed. Engl.* **1972**, *11*, 1020–1021; *Angew. Chem.* **1972**, *84*, 1099.
[17] J. H. Holloway, D. Laycock, in *Advances in Inorganic Chemistry*, Elsevier, **1984**, pp. 73–99.
[18] Yu. A. Buslayev, Yu. V. Kokunov, V. A. Bochkaryova, E. M. Shustorovich, *J. Inorg. Nucl. Chem.* **1972**, *34*, 2861–2865.
[19] Y. A. Buslaev, Y. V. Kokunov, V. A. Bochkareva, *Russ. J. Inorg. Chem.* **1972**, *17*, 1774.
[20] G. E. Blokhina, I. N. Belyaev, A. A. Opalovskii, L. I. Belan, *Russ. J. Inorg. Chem.* **1972**, *17*, 1113.
[21] Y. A. Buslaev, Y. V. Kokunov, V. A. Bochkareva, E. M. Shustorovich, *Dokl. Akad. Nauk SSSR* **1971**, *201*, 925.
[22] Y. A. Buslaev, A. A. Kuznetsova, S. V. Bainova, Y. V. Kokunov, *Koord. Khim.* **1977**, *3*, 216.
[23] B. F. Hoskins, A. Linden, T. A. O'Donnell, *Inorg. Chem.* **1987**, *26*, 2223–2228.
[24] M. Hamadène, F. Balegroune, A. Guehria-Laïdoudi, J. Grannec, J. Ravez, *J. Chem. Crystallogr.* **2006**, *36*, 1–5.
[25] C. Mühle, A. Karpov, A. Verhoeven, M. Jansen, *Z. Anorg. Allg. Chem.* **2005**, *631*, 2321–2327.
[26] F. Hiltmann, P. Zum Hebel, A. Hammerschmidt, B. Krebs, *Z. Anorg. Allg. Chem.* **1993**, *619*, 293–302.
[27] R. E. Stene, B. Scheibe, C. Pietzonka, A. J. Karttunen, W. Petry, F. Kraus, *J. Fluorine Chem.* **2018**, *211*, 171–179.
[28] J mol: An Open-Source Java Viewer for Chemical Structures in 3D. http://www.J mol.Org/, **n.d**.
[29] J. A. A. Ketelaar, C. Haas, J. van der Elsken, *J. Chem. Phys.* **1956**, *24*, 624–625.
[30] A. A. Opalovskii, T. D. Fedotova, *Russ. Chem. Rev.* **1970**, *39*, 1003–1016.
[31] A. Ažman, A. Ocvirk, D. Hadži, P. A. Giguère, M. Schneider, *Can. J. Chem.* **1967**, *45*, 1347–1350.
[32] A. Beuter, W. Sawodny, *Z. Anorg. Allg. Chem.* **1976**, *427*, 37–44.
[33] J. J. Rush, L. W. Schroeder, A. J. Melveger, *Chem. Phys. Lett.* **1970**, *6*, 533–536.
[34] *X-Area*, STOE & Cie GmbH, Darmstadt, Germany, **2011**.
[35] G. M. Sheldrick, *Acta Crystallogr. Sect. A Acta Crystallogr. Sect. A: Found. Crystallogr.* **2008**, *64*, 112–122.
[36] G. M. Sheldrick, *Acta Crystallogr. Sect. A Acta Crystallogr. Sect. C: Struct. Chem.* **2015**, *71*, 3–8.
[37] H. Putz, K. Brandenburg, *Diamond - Crystal and Molecular Structure Visualization*, Crystal Impact, Bonn, Germany, **2015**.
[38] *STOE WinXPOW*, STOE & Cie GmbH, Hilpertstrasse 10, 64295 Darmstadt, Germany, **2015**.
[39] *OPUS*, Bruker Optik GmbH, Ettlingen, Germany, **2009**.
[40] J. P. Perdew, K. Burke, M. Ernzerhof, *Phys. Rev. Lett.* **1996**, *77*, 3865–3868.
[41] C. Adamo, V. Barone, *J. Chem. Phys.* **1999**, *110*, 6158–6170.
[42] F. Weigend, R. Ahlrichs, *Phys. Chem. Chem. Phys.* **2005**, *7*, 3297.
[43] S. I. Ivlev, A. J. Karttunen, R. Ostvald, F. Kraus, *Z. Anorg. Allg. Chem.* **2015**, *641*, 2593–2598.
[44] A. J. Karttunen, T. Tynell, M. Karppinen, *J. Phys. Chem. C* **2015**, *119*, 13105–13114.
[45] S. Ivlev, V. Sobolev, M. Hoelzel, A. J. Karttunen, T. Müller, I. Gerin, R. Ostvald, F. Kraus, *Eur. J. Inorg. Chem.* **2014**, *2014*, 6261–6267.
[46] R. Dovesi, A. Erba, R. Orlando, C. M. Zicovich-Wilson, B. Civalleri, L. Maschio, M. Rérat, S. Casassa, J. Baima, S. Salustro, et al., *Wiley Interdiscip. Rev. Comput. Mol. Sci.* **2018**, e1360.
[47] C. M. Zicovich-Wilson, F. Pascale, C. Roetti, V. R. Saunders, R. Orlando, R. Dovesi, *J. Comput. Chem.* **2004**, *25*, 1873–1881.
[48] F. Pascale, C. M. Zicovich-Wilson, F. López Gejo, B. Civalleri, R. Orlando, R. Dovesi, *J. Comput. Chem.* **2004**, *25*, 888–897.
[49] L. Maschio, B. Kirtman, M. Rérat, R. Orlando, R. Dovesi, *J. Chem. Phys.* **2013**, *139*, 164101.
[50] L. Maschio, B. Kirtman, M. Rérat, R. Orlando, R. Dovesi, *J. Chem. Phys.* **2013**, *139*, 164102.

Received: May 27, 2019

